ISBN-82553-0596-3 No 1
Applied Mathematics 1986

NUMERICAL SOLUTION OF THE THREE DIMENSIONAL BOUSSINESQ EQUATIONS FOR DISPERSIVE SURFACE WAVES PART 2

by

Geir Pedersen & Ole B. Rygg

PREPRINT SERIES - Matematisk institutt, Universitetet i Oslo

ABSTRACT

This is the second part of the documentation of a numerical method solving the three dimensional Boussinesq equation. We are mainly consentraiting on numerical tests of the method already presented, but a treatment of the nonlinear Boussinesq equation is also suggested.

Results for eigenoscillations in basins with variable depth in one direction are compared to numerical results obtained from a shooting method. The agreement is excellent.

The method have with promising results been used on the three dimensional refraction/diffraction problem.

To test the extension to nonlinear problems two different cases have been investigated. The first is the propagation of a solitary wave and the second is a three dimensional nonlinear initialvalue problem in a basin. Both tests turned out nicely.

CONTENTS

1. INTRODUCTION

Introductory remarks

This preprint is the second part of "Numerical solution of the three dimensional Boussinesq equations for dispersive surface waves". While the first part mainly contained analysis of schemes and iteration procedures in the linear case, the second deals with both linear and non-linear test examples.

For practical reasons numeration of the chapters in the present part starts from 1. To avoid confusion, equations and figures in the first part are therefor referred to by the roman digit I. As an example we denote the sixt equation of chapter 2 in part one by (I;2.6) while the correspondingly situated equation in the second part is referred to as (2.6). Most notations used in part one is maintained unaltered. The few differences that are present are dealt with in the next paragraph.

In part one vectorial quantities were recognized by arrows. Here we instead write them in bold face. In pharagraph 2.1 of part one numerical averaging operations were defined. In the present part we sometimes applies two such operations to the same quantity. In these cases we write a single overbar and list the appropriate coordinates behind it. As an example: the average of u with respect to both y and t is denoted by $\bar{u}^{y,t}$. We note that the averaging operators are comutative. The sequential order of the coordinates is thus arbitrary.

2. EIGEN-OSCILLATIONS IN BASINS.

In chapter 3.3 of part 1 eigen-oscillations in a rectangular basin of constant depht where used as test examples. We are now going to generalize by allowing for depth variations in the x-direction only. The y-dependence can still be assumed to be sinusoidal and the equations are still seperable in x,y and t. Hence the eigen-oscillation solutions may be expressed:

$$(u,\eta) = (\ \hat{u}(x), \hat{\eta}(x)\ ) e^{i\omega t} \cos l_n y \qquad v = \hat{v}(x) e^{i\omega t} \sin l_n y$$

After the y and t dependence are seperated off, the remaining eigenvalue problem is solved by a shooting technique as described in appendix A. Initial conditions extracted from these solutions are then implemented in the finite difference scheme and comparison of time series are made.

We are going to investigate two test examples. In both examples the basin is confined to $(0 < x < 3 \quad , \quad 0 < y < 4)$, the grid increments all equal 0.5 and the reported time series correspond to the surface elevation at $x = 0.5 \quad y = 1$ relative to the maximum value of the $\hat{\eta}$. All space coordinates are scaled equally to give "$\epsilon = 1$". For initiation of the iterations, values from the previous time step are used.

Example 1: Linear bottom topography. The bottom function h equals $\frac{1}{2} + \frac{1}{3}x$. By the method described in appendix A we find $\omega_{1,1} = 1.02$ (the interpretation of the subscripts is given in the appendix) and $\hat{u}$,$\hat{v}$ and $\hat{\eta}$ as depicted in figure 2.2(a),2.2(b) and 2.2(c) respectively. Time series of η are depicted in figure 2.3. The "shooting solution" corresponds to full drawn lines, the solution of the difference scheme to the marks. The results obtained by using one iteration/no relaxation , two iterations/no relaxation and one iteration/relaxation are reported in (a),(b) and (c) respectively. The relaxation factors r_x and r_y (defined in chapter 3 , part 1) are chosen as $\frac{\pi^2}{48}$ and $\frac{\pi^2}{27}$. This choice would optimize the convergence of a wave with wavenumber vector $\frac{2\pi}{3}\mathbf{i} + \frac{2\pi}{8}\mathbf{j}$ in a basin of constant depth equal to 1. Using two iterations we get very good agreement. Most of the small deviations which are present are probably due to the small number of gridpoints used. One iteration without relaxation gives a severe amplification. One iteration with relaxation works on the other hand almost as well as two itrations/no relaxation.

Example 2: Similar to example 1 except from the depth which is given by $h = 1 + \frac{1}{2}\sin\pi(\frac{1}{3}x - \frac{1}{2})$. The important point is that this bottom function has a non-zero second derivative. In this case we have $\omega_{1,1} = 1.004$. The eigenoscillation amplitude functions $\hat{u}$, $\hat{v}$ and $\hat{\eta}$ are depicted in figure 2.4 and the time series in figure 2.5. All notations, sequential

arrangments etc. equals those of the previous example. The agreement is approximately as in the first example.

Conclusion: The present results indicate that two iterations at each time step generally suficce even for relatively short waves and that relaxation may be useful also in the case of variable depth.

3. REFRACTION AND DIFFRACTION OF PERIODIC WAVES

In this chapter we are going to use the linear Boussinesq equations to study refraction and diffraction of periodic waves. The basic equations are (1.1), (1.5) and (1.6) of part 1.
A channel of finite width is assumed, bounded by side-walls which completely reflects the waves. We allow depth variations both in x- and y- direction, except in the vicinity of open boundaries.

3.1 Boundary conditions

At a rigid wall we have the boundary condition $\mathbf{v} \cdot \mathbf{n} = 0$, where $\mathbf{n}$ is a normal to the boundary. This reflection condition has been imposed on the side-walls of the channel, figure 2.1. The difference approximation for this condition appropriate for our test examples is

$$v^n_{i+\frac{1}{2},j} = 0$$
$$\delta_y u^n_{i,j} = 0$$

We assume a plane wave-train incident on the left side of the channnel:

$$u = A \sin(kx - \omega t) \tag{3.1}$$

where A is the amplitude of the incoming wave. At the right boundary we want to avoid reflection. We therefore take the radiation condition:

$$\frac{\partial u}{\partial t} + c\frac{\partial u}{\partial x} = 0 \tag{3.2}$$

where c is the phase velocity obtained from the dispersion relation for the Boussinesq equations. With a considerable depth variation in the channel reflected waves may have a significant amplitude. It is therefore desirable to let the reflected waves escape at the left boundary. When we just specify the velocity at the left boundary, equation (3.1), this boundary operate as a rigid wall for reflected waves. If we combine (3.1) with a radiation condition for waves propagating to the left,

$$\frac{\partial u}{\partial t} - c\frac{\partial u}{\partial x} = 2\omega A \cos(kx - \omega t) \tag{3.3}$$

we have an inhomogenous boundary condition which both radiate and generate waves (Rygg 1985).
The difference approximation of the conditions (3.1), (3.2) and (3.3) are accordingly:

$$u^n_{j+\frac{1}{2}} = A\sin\{k(j+\frac{1}{2})\triangle x - \omega n\triangle t\} \tag{3.4}$$

$$[\delta_t \bar{u}^x + c\delta_x \bar{u}^t = 0]^n_{j+\frac{1}{2}} \tag{3.5}$$

$$[\delta_t \bar{u}^x - c\delta_x \bar{u}^t]^n_{j+\frac{1}{2}} = A\{-\Omega\cos(\frac{k\triangle x}{2}) - cK\cos(\frac{\omega\triangle t}{2})\}\cos\{k(j+\frac{1}{2})\triangle x - \omega n\triangle t\} \tag{3.6}$$

The choice of central differences in the boundary conditions is based on numerical tests.
All the above boundary conditions are formulated for wavetrains propagating normal to the open boundary. With depth variations in the channel this is not the case. The reflection coefficient (ratio between amplitude of reflected and incomming waves) for a wave propagating through an open boundary with angle of incidence α is :

$$R = \frac{c_B - c_x}{c_B + c_x} \tag{3.7}$$

c_B is the phase velocity used in the boundary condition (3.2) and c_x is the x-component of the phase velocity of the incomming wave, figure 3.1. Considering the shallow water equation (omitting the dispersion term in the Boussinesq equation) we may write:

$$R = \frac{\cos\alpha - 1}{\cos\alpha + 1} \tag{3.8}$$

For $\alpha = 45^0$ we have a reflection coefficient $R = 0.17$. This indicate that waves within an angle of incidence of 45 degrees produces a reflected wave with amplitude less than 17 percent of the incoming wave. Based on this crude analysis we may though accept the normal boundary condition for waves with an angle of incidence up to 45 degrees. The test cases in this chapter fullfill these requests.

3.2 Two-dimensional depth-variation in a channel

We assume plane progressive waves propagating through a channel along the x-axis. Depth variations is allowed in the x-direction only. The problem then reduces to a two-dimensional one.
The two-dimensional linear Boussinesq equation has the form:

$$\frac{\partial \eta}{\partial t} = -\frac{\partial}{\partial x}(hu) \tag{3.9}$$

$$\frac{\partial u}{\partial t} = -\frac{\partial \eta}{\partial x} + \frac{h}{2}\frac{\partial^2}{\partial x \partial t}[\frac{\partial}{\partial x}(hu)] - \frac{h^2}{6}\frac{\partial^3 u}{\partial^2 x \partial t} \tag{3.10}$$

The difference approximation for these equations reads:

$$[\delta_t \eta = -\delta_x(hu)]^{n+\frac{1}{2}}_{j+\frac{1}{2}} \tag{3.11}$$

$$[\delta_t u = -\delta_x \eta + \frac{h}{2}\delta_t \delta_x^2(hu) - \frac{h^2}{6}\delta_t \delta_x^2 u]^n_j \tag{3.12}$$

The last equation is implicit in the velocity u. This gives rise to a tridiagonal set of linear equations, which can easely be solved by a Gaussian elimination.
We choose the depth variation as a parabolic half cylinder situated at the bottom of the channel, figure 3.2(a). The shape of the cylinder exhibit from the relation:

$$h = 1 - A[1 - \frac{x^2}{R^2}] \tag{3.13}$$

where A is the maximum height of the cylinder, and R is half the width of the cylinder. At the left boundary we used the combined radiation and generating boundary condition, equation 3.6, and at the right boundary the radiation condition, equation 3.5. Characteristic parameters for our simulation was:

$$\omega = 0.71767 \qquad A = 0.7 \qquad R = 2.0$$

This corresponds to a wavelength of about 8 times the depth. Figure 3.2(b) gives the surface displacement η in the channel evaluated with the Boussinesq equation. In figure 3.2(c) we compare the maximum surface displacement over one periode for three different equations. The three equations are, the linear Boussinesq equation, the linear shallow water equation, and the mild-slope equation. As depicted in figure 2a of part 1 the shallow water equation has an error in the dispersion relation of about 10 percent for wavelengths 8 times the depth. Accordingly it is not unexpected that the shallow water equations overestimate both the reflection from the shoal and the increase in surface displacement on top of the shoal.
The mild-slope equation gives about the same surface displacement over the shoal as the Boussinesq equation, but the slope of the shoal is higher than the validity limit for the

mild-slope equation. Reflections from the shoal are for that reason markedly greather than predicted by the Boussinesq equation.

3.3 Wave focusing by a circular shoal

In the three-dimensional test case, we are studying propagation of incident plane waves over a circular symmetric shoal with parabolic bottom profile. The shoal is represented by the depth profile:

$$h = 1 - A[1 - (\frac{x^2 + y^2}{R^2})] \tag{3.14}$$

where A is the maximum height of the shoal, R is the radius of the shoal, and x,y is the distance from the center of the shoal in x- and y-direction respectively. The basic equations are the linear Boussinesq equations (I;1.1 and I;1.5-I;1.6) with difference approximations exhibited in equation (I;2.6 - I;2.9). The iteration procedure for this numerical scheme is discussed in chapter 3 of part 1.

In section 3.1 several boundary conditions where discussed. For the three-dimensional problem we take the normal radiation condition, equation (3.5), and the generating condition, equation (3.4), for u (the velocity in x-direction). Fictive quantities outside the left and right boundary must be specified for v, the velocity in y-direction. This is obtained from the irrotaional condition (I;1.4). The suitable numerical approximation reads:

$$[\delta_x v = \delta_y u]^n_{i,j} \tag{3.15}$$

Solving the implicit equations for each time step by the iterative procedure is the time-consuming operation. It is therefore desirable to reduce the number of iterations. Hence we make effort to minimize the damping factors β_x and β_y (equation I;3.9) for the dominant wavelengths. Equation (I;3.9) determine the relaxations factors r_x and r_y respectively. Characteristic parameters for our test example was :

$$\omega = 0.71767 \qquad A = 0.7 \qquad R = 2.0$$

$$\Delta t = 0.5 \qquad \Delta x = 0.5 \qquad \Delta y = 0.2$$

This corresponds to a wavelength of about 8 times the characteristic depth. The length of the channel is $40\Delta x$ and the total width is $48\Delta y$. We utilize the symmetry in the channel and evaluate for half the channel width. At the line of symmetry a reflection condition has

been imposed. 275 time step was simulated ($\sim$ 16 periods) before a periodic situation was assumed.

Figure 3.3(a) shows the bottom profile. In figure 3.3(b) the surface displacement at a point of time is depicted. The wave focusing behind the shoal is viewed in figure 3.3(c), where the maximum surface displacement for one periode is plotted. Figure 3.4 compare the focusing effect evaluated with the Boussinesq equations and the shallow water equations. The figure show the maximum surface displacement at the centerline in the channel. The tendency of overestimating the reflection, as discussed in section 3.2, is distinct also in this example.

In this test simulation we used four iterations. Two of them with relaxation. The relaxation factor was obtained choosing the Nyquist wavelength as the dominant wavelength. The depth profile has in this test a discontinuity in the first derivative (see Figure 3.1(a)). This gives rise to problems in the dispersion term in the Boussinesq equation where second order derivatives of h appear. The resulting noise seems to be accumulative and becomes visible after a number of time steps. This number is increased by applying more iterations with relaxation. Hence the growth of the noise must be assumed to stem from the initiation of the iteration procedure. If smoothing or another modifications is applied to initials values the problem is probably avoided without increasing the number of iterations. As shown in this test the growth is fairly slow and four iterations with relaxation is for most cases sufficient.

4. NONLINEARITIES

4.1 The nonlinear formulation of the Boussinesq-equations.

The nonlinear Boussinesq-equations corresponding to (I;1.1) and(I;1.2) reads:(Peregrine 1972)

$$\frac{\partial \eta}{\partial t} = -\nabla \cdot ((h+\eta)\mathbf{v}) \tag{4.1}$$

$$\frac{\partial \mathbf{v}}{\partial t} + \mathbf{v} \cdot \nabla \mathbf{v} = -\nabla \eta + \epsilon \mathbf{D}(\frac{\partial \mathbf{v}}{\partial t}) + o(A\epsilon^2, \epsilon A^2) \tag{4.2}$$

where A is an amplitude and $\mathbf{D}$ is the differensial operator which gives the dispersion terms. Equation (4.1) is valid for amplitudes A of order ϵ. Hence the nonlinear terms may be rewritten by use of the irrotational requirement (I;1.4). From (4.2) we get:

$$\dot{u} + \frac{\partial}{\partial x}(\frac{1}{2}\mathbf{v}^2) = -\frac{\partial \eta}{\partial x} + \epsilon D_x + o(A\epsilon^2) \tag{4.3}$$

$$\dot{v} + \frac{\partial}{\partial y}(\frac{1}{2}\mathbf{v}^2) = -\frac{\partial \eta}{\partial y} + \epsilon D_y + o(A\epsilon^2) \tag{4.4}$$

where D_x and D_y are the components of the dispersion terms.

4.2 Numerical representation of the nonlinearities.

A mid-point difference approximation to (4.1) corresponding to (I;2.6) is given by:

$$[\delta_t \eta = -\delta_x\{(h+\bar{\eta}^{x,t})u\} - \delta_y\{(h+\bar{\eta}^{y,t})v\}]^{n-\frac{1}{2}}_{j+\frac{1}{2},p+\frac{1}{2}} \tag{4.5}$$

This is a coupled set of equations for η^n which has to be solved by an iterative method. A number of line by line methods may be formulated for this spesific problem. However, in this report we will examinate a simpler approach. Predictor values for η^n , referred to as $\tilde{\eta}^n$, are obtained by:

$$[\frac{1}{\Delta t}(\tilde{\eta}^n - \eta^{n-1}) = -\delta_x\{(h+(\bar{\eta}^x)^{n-1})u^{n-\frac{1}{2}}\} - \delta_y\{(h+(\bar{\eta}^y)^{n-1})v^{n-\frac{1}{2}}\}]_{j+\frac{1}{2},p+\frac{1}{2}} \tag{4.6}$$

Substitution of $\eta_*^{n-\frac{1}{2}} \equiv \frac{1}{2}(\tilde{\eta}^n + \eta^{n-1})$ for $(\bar{\eta}^t)^{n-\frac{1}{2}}$ in (4.5) gives an expression for corrected values for η^n :

$$[\delta_t \eta = -\delta_x\{(h + \bar{\eta}_*^x)u\} - \delta_y\{(h + \bar{\eta}_*^y)v\}]_{j+\frac{1}{2},p+\frac{1}{2}}^{n-\frac{1}{2}} \tag{4.7}$$

Equation (4.6) and (4.7) may be interpreteted as two Jacobi iterations applied to the implicit equation (4.5) with η^{n-1} as initial values. This method will work well as long as the linear set of equations defined by (4.5) is strongly diagonal dominant. If u becomes comparable to the wavespeed the diagonal dominance is weakened and other methods may be advantagous. In the two dimensional case we have compared the performance of (4.6) and (4.7) to the performance of the fully implicit equation (4.5) (see section 4.3).
To construct the nonlinear versions of (I;2.7) and (I;2.8) we have to assign values to $\frac{\partial}{\partial x}\mathbf{v}^2$ and $\frac{\partial}{\partial y}\mathbf{v}^2$ at $(j\triangle x, (p+\frac{1}{2})\triangle y, n\triangle t)$ and $((j+\frac{1}{2})\triangle x, p\triangle y, n\triangle t)$ respectively. Geometrical averaging applied to velocities at $t = (n+\frac{1}{2})\triangle t$ and $t = (n-\frac{1}{2})\triangle t$ gives:

$$(u^{(n)})^2 = (u^{(n-\frac{1}{2})})^2 + \triangle t u^{n-\frac{1}{2}} \dot{u}^n + o(\triangle t^2) \tag{4.8}$$

Averaging in space then leads to:

$$\begin{aligned} \frac{1}{2}\mathbf{v}^2((j+\frac{1}{2})\triangle x, (p+\frac{1}{2})\triangle y, n\triangle t) = \frac{1}{2}[\{(\bar{u}^x)^{(n-\frac{1}{2})}\}^2 + \{(\bar{v}^y)^{(n-\frac{1}{2})}\}^2 \\ + \triangle t((\bar{u}^x)^{n-\frac{1}{2}}(\dot{\bar{u}^x})^n + (\bar{v}^y)^{n-\frac{1}{2}}(\dot{\bar{v}^y})^n)]_{j+\frac{1}{2},p+\frac{1}{2}} \\ + o(\triangle t^2, \triangle x^2, \triangle y^2) \\ \equiv T^n_{j+\frac{1}{2},p+\frac{1}{2}} + o(\triangle t^2, \triangle x^2, \triangle y^2) \end{aligned} \tag{4.9}$$

The difference form of (4.3) and (4.4) may then be written:

$$\begin{aligned} 0 &= [\dot{u} + \delta_x(\eta + T) - \epsilon D_x]^n_{j,p+\frac{1}{2}} \\ 0 &= [\dot{v} + \delta_y(\eta + T) - \epsilon D_y]^n_{j+\frac{1}{2},p} \end{aligned} \tag{4.10}$$

where the representation of D_x and D_y is the same as in (I;2.7). We note that (4.10) still is a set of linear equations for the accelerations. In two dimensions we have also tested a leap-frog like representation of the nonlinearity:

$$0 = [\dot{u} + \delta_x \eta - \epsilon D_x]^n_j + \frac{1}{2\triangle x}(T^n_{j+1} - T^n_{j-1}) \tag{4.11}$$

where

$$T_j^n = \frac{1}{2}(u_j^{(n-\frac{1}{2})})^2 + \frac{1}{2}\Delta t u_j^{n-\frac{1}{2}} \dot{u}_j^n \tag{4.12}$$

4.3 Propagation of a solitary wave.

In the previous section two different difference schemes was suggested for the continuity equation (equation 4.5 and equation 4.6). Although equation (4.5) is implicit it reduces to a tridiagonal matrix in the two-dimensional case. The nonlinear velocity term may be represented by equation (4.10) or equation (4.11). We have consequently four possibilities for implementation.

As a suitable test for the numerical approximation we use the propagation of a solitary wave. This stationary wave-solution is deduced in appendix B. The shape and the phase velocity remains constant when the solitary wave propagates on constant depth. We investigate the solitary wave after a certain distance is covered. In table 4.1 we compare the maximum surface displacement and the corresponding phase velocity evaluated with the four different numerical schemes. It is evident from this table that the predictor-corrector evaluation of the surface displacement in combination with equation (4.11) is the best choice.

We now consider the propagation of a solitary wave over a shelf (figure 4.1 a). As the depth vary the shape of the solitary wave change. Figure 4.1 (b)-(d) depict three different stages of the propagation. The figures displays splitting of the solitary wave which is well known from the literature.

4.4 A three-dimensioanal nonlinear initialvalue problem.

An initial-value problem is solved by three different sets of equations: (i) The linear shallow water equations. (ii) The linearized Boussinesq equations. (iii) The non-linear Boussinesq equations. A rectangular basin of constant depth equal to 1 is confined to $0 < x < L$, $0 < y < B$. At $t = 0$ we specify the surface elavation and the velocities equals zero. To start the time integrating procedure we need values for the velocities at $t = -\frac{1}{2}\Delta t$. Firstly the accelerations at $t = 0$ are found from the momentum equation by using a large number of iterations. Even in the nonlinear case this can be done by substituting 0 for T in (4.10). Secondly the velocities at $t = -\frac{1}{2}\Delta t$ are found by demanding: $u_{\ldots}^{-\frac{1}{2}} + u_{\ldots}^{\frac{1}{2}} = 0 \quad v_{\ldots}^{-\frac{1}{2}} + v_{\ldots}^{\frac{1}{2}} = 0$. The shape of the initial disturbance is given by:

$$\eta(x, y, 0) = A(1 + \cos(\frac{\pi y}{B})) \cosh^{-2} \alpha x$$

Choosing $A = 0.25 \quad \alpha = 0.30625 \quad B = 8 \quad L = 40$ and integrating to $t = 30$ we get the results depicted in figure 4.2 and 4.3. From the figures we can deduce that both dispersional effects and non-linearities are important in this example. The grid refinement tests shows that good accuracy is obtained by choosing $\Delta x = \Delta y = \Delta t = 1.0$. It is also clear that two iterations are sufficient in this case.

5. CONCLUDING REMARKS

The two parts of the preprint "Numerical solution of the three dimensional Boussinesq equations for dispersive surface waves" should provide a good basis for applications and further development of the method. Both the scheme itself and the iteration procedure have been subjected to normal mode analyzis in the case of constant coefissients. The outcome of the analyzis is indeed satisfactory. More complex tests involving variable depth, open boundaries and nonlinearities have given resonable and very promising results. Though the development of the method has by no means been carried out to an ultimate level. Better radiation conditions should be formulated (as always) and effective ways of implementing irregular boundaries must be found. In addition the treatment of the nonlinearities is no more than a first premature attempt, even though it so far seems quite sucessful. Elimination of the short comings of the method in its present form is left to be done as parts of applying it.

APPENDIX A.

A shooting method for eigen-oscillations in basins.

A rectangular basin is defined by $0 < x < L$, $0 < y < B$. At the boundaries the normal component of the velocity equals zero. If the depth ,h, is independent of y the eigen-oscillation solutions are separable:

$$(u, \eta) = (\hat{u}(x), \hat{\eta}(x))e^{i\omega t} \cos l_n y \qquad v = \hat{v}(x)e^{i\omega t} \sin l_n t \qquad (A-1)$$

where the values of $l_n = \frac{n\pi}{B}$ are obtained from the boundary conditions at $y = 0$ and $y = B$. Substitution of (A-1) into (I;1.1) , (I;1.5) and (I;1.6) gives:

$$i\omega\hat{\eta} = -(h\hat{u})' - l_n h\hat{v} \qquad (A-2)$$

$$i\omega\hat{u} = -\hat{\eta}' + i\omega\epsilon h[\frac{1}{2}(h\hat{u})'' - \frac{1}{6}h\hat{u}'' - \frac{1}{3}hl_n^2\hat{u} + \frac{1}{2}l_n h'\hat{v}] \qquad (A-3)$$

$$i\omega\hat{v} = l_n\hat{\eta} + i\omega\epsilon h[\frac{1}{2}(h\hat{v}')' - \frac{1}{6}h\hat{v}'' - \frac{1}{3}hl_n^2\hat{v}] \qquad (A-4)$$

Using (A-2) to eliminate $\hat{\eta}$ we get two coupled second order equations for $\hat{u}$ and $\hat{v}$:

$$(1 - \frac{1}{3}\sigma h)h\hat{u}'' + (1 - \sigma h)h'\hat{u}' + (\omega^2 + h'' - \sigma h\{\frac{1}{2}h'' - \frac{1}{3}l_n^2 h\})\hat{u} + l_n h\hat{v}' + (1 - \frac{1}{2}\sigma h)l_n h'\hat{v} = 0 \qquad (A-5)$$

$$\frac{1}{3}\sigma h^2\hat{v}'' + \frac{1}{2}\sigma hh'\hat{v}' - (\omega^2 - l_n^2 h + \frac{1}{3}\sigma h^2 l_n^2)\hat{v} + l_n h\hat{u}' + l_n h'\hat{u} = 0 \qquad (A-6)$$

where $\sigma = \epsilon\omega^2$. From (A-6) and the irrotational condition we easily obtain:

$$\hat{v} = [(l_n h - \frac{1}{3}\sigma h^2 l_n)\hat{u}' + (l_n h' - \frac{1}{2}\sigma hh' l_n)\hat{u}][\omega^2 - l_n^2 h + \frac{1}{3}\sigma h^2 l_n^2]^{-1} + o(\epsilon^2) \qquad (A-7)$$

Within the accuracy of the Boussinesq equations this expression may be substituted for $\hat{v}$ in (A-5) to give a single second order equation for $\hat{u}$. However, our intension is to use the eigen-oscillation solutions as test examples for the numerical scheme. Hence we solve (A-5) and (A-6) which are completely consistent with (I;1.1) , (I;1.5) and (I;1.6) . At the boundaries $x = 0$ and $x = L$ we have the zero flux conditions $\hat{u}(0) = \hat{u}(L) = 0$. In addition we use the symmetriy conditions: $\hat{v}'(0) = \hat{v}'(L) = 0$. These conditions completes the problem by specifying the rotations to be of order ϵ. The eigen-solutions of (A-5) and (A-6) may be written:

$$\hat{u} = A\hat{u}_1(x,\omega) + B\hat{u}_2(x,\omega) \qquad \hat{v} = A\hat{v}_1(x,\omega) + B\hat{v}_2(x,\omega) \qquad (A-8)$$

where the pairs $\hat{u}_1, \hat{v}_1$ and $\hat{u}_2, \hat{v}_2$ are solutions of (A-5) and (A-6) satisfying the initial conditions $\hat{u}_1 = \hat{v}_1 = \hat{v}_1' = 0$, $\hat{u}_1' = 1$ and $\hat{u}_2 = \hat{u}_2' = \hat{v}_2' = 0$, $\hat{v}_2 = 1$ at $x = 0$. A non-trivial solution of the form (A-8) which also satisfy the conditions at $x = L$ exists only if:

$$0 = D(\omega) \equiv (\hat{u}_1\hat{v}_2' - \hat{u}_2\hat{v}_1') \mid_{x=L} \qquad (A-9)$$

For a given ω , $D(\omega)$ is found by integrating (A-5) and (A-6) from $x = 0$ to $x = L$ by a Runge-Kutta technique and substituting the resulting values for $\hat{u}_1, \hat{u}_2, \hat{v}_1', \hat{v}_2'$ into the rigthmost side of (A-9). The equation $D(\omega) = 0$ is solved by a secant method. For each l_n there exists an infinite number of eigen-values ω which are denoted by $\omega_{m,n}$ $(m = 0, 1, 2...)$ in increasing order.

APPENDIX B.

The solitary wave solution

In the two-dimensioanal case a stationary wave-solution may be written:

$u = U(x-ct) \quad \eta = Y(x-ct)$. Substitution of these expressions into the two-dimensional versions of (4.1) and (4.3) gives a set of two ordinary differential equations:

$$cY' = ((1+Y)U)' \qquad (B-1)$$

$$(U-c)U' = -Y' - \frac{\epsilon}{3}cU''' \qquad (B-2)$$

The depth has been set equal to 1 and the phase speed c has to be found as a part of the solution. A single crested wave solution must be found from (B-1),(B-2) and the condition of vanishing amplitude at infinity:

$$\lim_{\xi \to \inf} U(\xi), Y(\xi), U'(\xi), Y'(\xi), \ldots = 0 \qquad (B-3)$$

Integration of (B-1) and (B-2) using condition (B-3) leads to:

$$Y = U(c-U)^{-1} \qquad (B-4)$$

$$\frac{1}{2}U^2 - cU = -Y - \frac{\epsilon}{3}cU'' \qquad (B-5)$$

Elimination of Y in (B-5) , multiplication by U' ,integration and use of (B-3) gives:

$$-\frac{1}{6}U^3 + \frac{1}{2}cU^2 + U + c\ln(1-\frac{U}{c}) = \frac{\epsilon}{6}c(U')^2 \qquad (B-6)$$

The maximum amplitude, U_0, is obtained when $U' = 0$. Hence we get the implicit relation for $c(U_0)$:

$$-\frac{1}{6}U_0^3 + \frac{1}{2}cU_0^2 + U_0 + c\ln(1-\frac{U_0}{c}) = 0 \qquad (B-7)$$

If we instead of U_0 introduce the maximum surface elevation $A = U_0(c - U_0)^{-1}$, this equation simplifies to the explicit relation:

$$c^2 = \frac{(1+A)^2[(1+A)\ln(1+A) - A]}{\frac{1}{3}A^3 + \frac{1}{2}A^2} \qquad (B-8)$$

Expansion of the left hand side of this equation in terms of powers of A leads to:

$$c^2 = 1 + A + o(A^2) \qquad (B-8)$$

which is a well known result.

FIGURE CAPTIONS

Figure 2.1

Scetch of a rectangular basin.
– : u -node, | : v -node, o : η -node.

Figure 2.2

Eigenoscillations in the case of a linear bottom profile, referred to as example 1 in chapter 2. $\hat{u}, \hat{v}$ and $\hat{\eta}$ are depicted as functions of x in (a), (b) and (c) respectively. One unit on the ordinate corresponds to the maximum value of $\hat{\eta}$.

Figure 2.3

Time series for η at $x = 0.5 \quad y = 1$ in the first example of chapter 2. The fully drawn lines correspond to the "shooting" solution, the marks to the solution obtained from the difference scheme.
The integration of the difference equations is performed using:

(a) - one iteration/no relaxation

(b) - two iterations/no relaxation

(c) - one iteration/relaxation as described in the chapter.

Figure 2.4

Analogue to figure 2.2 for example 2 in chapter 2. (sinusoidal bottom profile)

Figure 2.5

Analogue to 2.3 for example 2. (sinusoidal bottom profile)

Figure 3.1

Reflection of a propagating wave with wave number $\mathbf{k} = k\mathbf{i} + l\mathbf{j}$.
α is the angle of incidence.

Figure 3.2

Plane periodic progressive waves. For simulation parameters see text.

a) The depth profile (see text)

b) The surface displacement η evaluated with the Boussinesq equation at a given point of time

c) The maximum surface displacement over one periode evaluated with three different equations: (—-) The Boussinesq equation, $(\cdots)$ The mild slope equation, and $(- \; - \; -)$ The shallow water equation.

Figure 3.3

Wave focusing by a circular shoal evaluated with the Boussinesq equation. Periodic progressive waves propagating from the left to the right.

a) Depth profile in the channel

b) The surface displacement η in the channel at a given point of time

c) The maximum surface displacement in the channel over one periode

Figure 3.4

The maximum surface displacement at the line of symmetry for the Boussinesq equation (——) and the Shallow water equation $(- \; - \; -)$.

Table 4.1

Amplitude of the solitary wave after propagating a specified distance.
($\triangle x = 0.5$, $\triangle t = 0.5$, $\eta_0 = 0.1$)

Figure 4.1

Propagation of a solitary wave over a shelf. ($\triangle x = 0.5$, $\triangle t = 0.5$, $\eta_0 = 0.1$)

a) The depth profile

b) Before reaching the shelf ($100\triangle t$)

c) Above the shelf ($150\triangle t$)

d) Propagation in the shallow region ($250\triangle t$)

Figure 4.2

Perspective plots of the surface elevation η.

(a) - initial elevation.

(b) - elevation at $t = 30$ found by integrating the nonlinear Boussinesq equations with $\Delta x = \Delta y = \Delta t = 1$.

(c) - elevation at $t = 30$ found by integrating the linear Boussinesq equations with $\Delta x = \Delta y = \Delta t = 1$.

(d) - elevation at $t = 30$ found by integrating the linear hydrostatic equations with $\Delta x = \Delta y = 1$ and $\Delta t = \frac{30}{43}$.

Figure 4.3

$\eta(x, 0, 30)$ as function of x for different choices of equations, grid increments and numbers of iterations. Three different grids are used for each equation.
(a) Results obtained from the nonlinear Boussinesq equation for $\Delta x = \Delta y = \Delta t = 1$. Fully drawn lines correspond to four iterations, marks to two iterations.
(b) Analogue to (a) for the linearized Boussinesq equations.
(c) Profiles obtained from the nonlinear Boussinesq equation. The fully drawn line corresponds to $\Delta x = \Delta y = \Delta t = 0.5$, the marks to $\Delta x = \Delta y = \Delta t = 1$. Two iterations are used in both cases.
(d) Analogue to (c) for the linearized Boussinesq equation.
(e) Profiles obtained from the hydrostatic equations. Fully drawn line corresponds to $\Delta x = \Delta y = 0.5 \quad \Delta t = \frac{30}{85}$, marks to $\Delta x = \Delta y = 1 \quad \Delta t = \frac{30}{43}$. The time step is chosen according to the stability requirement $\Delta t < (\Delta x^{-2} + \Delta y^{-2})^{-1}$ which is stronger than the stability requirement for the Boussinesq equation.
(f) Results from integration of the nonlinear Boussinesq equation . The fully drawn line corresponds to $\Delta x = \Delta y = \Delta t = 0.5$, the marks to $\Delta x = \Delta y = \Delta t = 2$. Two iterations are used in both cases. For $x < 20$ we have an instability which may be removed by choosing smaller time increments. (see (g)) It is not cured by increasing the number of iterations.
(g) Same as (f) apart from a halvation of the time increment assosiated with the marks. The instability is removed, but we get a poorer approximation to the leading pulse.
(h) Analogue to (f) for the linearized Boussinesq equation. No instability is revealed.
(i) Results obtained from the hydrostatic equations. The fully drawn line corresponds to $\Delta x = \Delta y = 0.5 \qquad \Delta t = \frac{30}{85}$, marks to $\Delta x = \Delta y = 2 \quad \Delta t = \frac{30}{22}$.

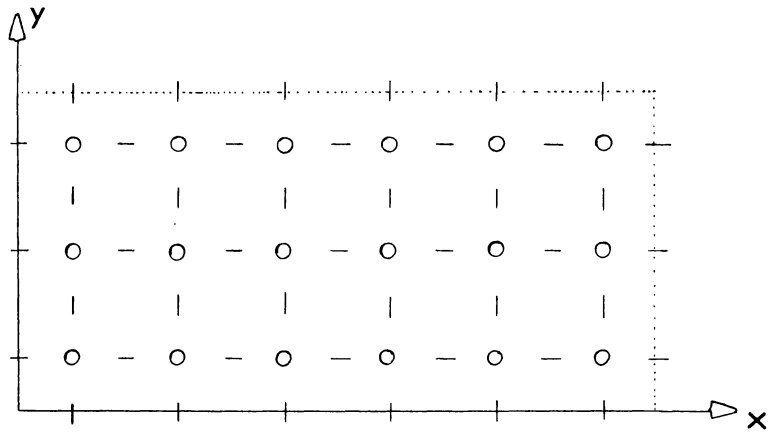

Figure 2.1

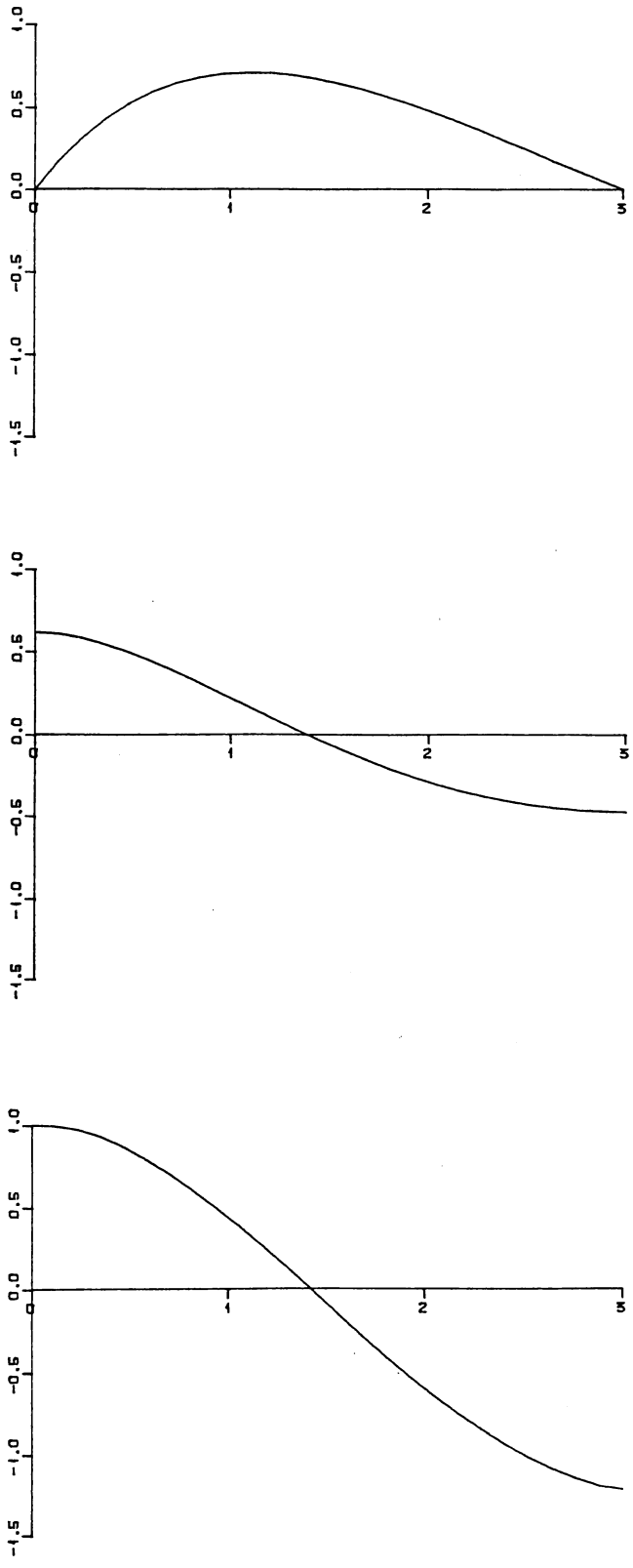

Figure 2.2

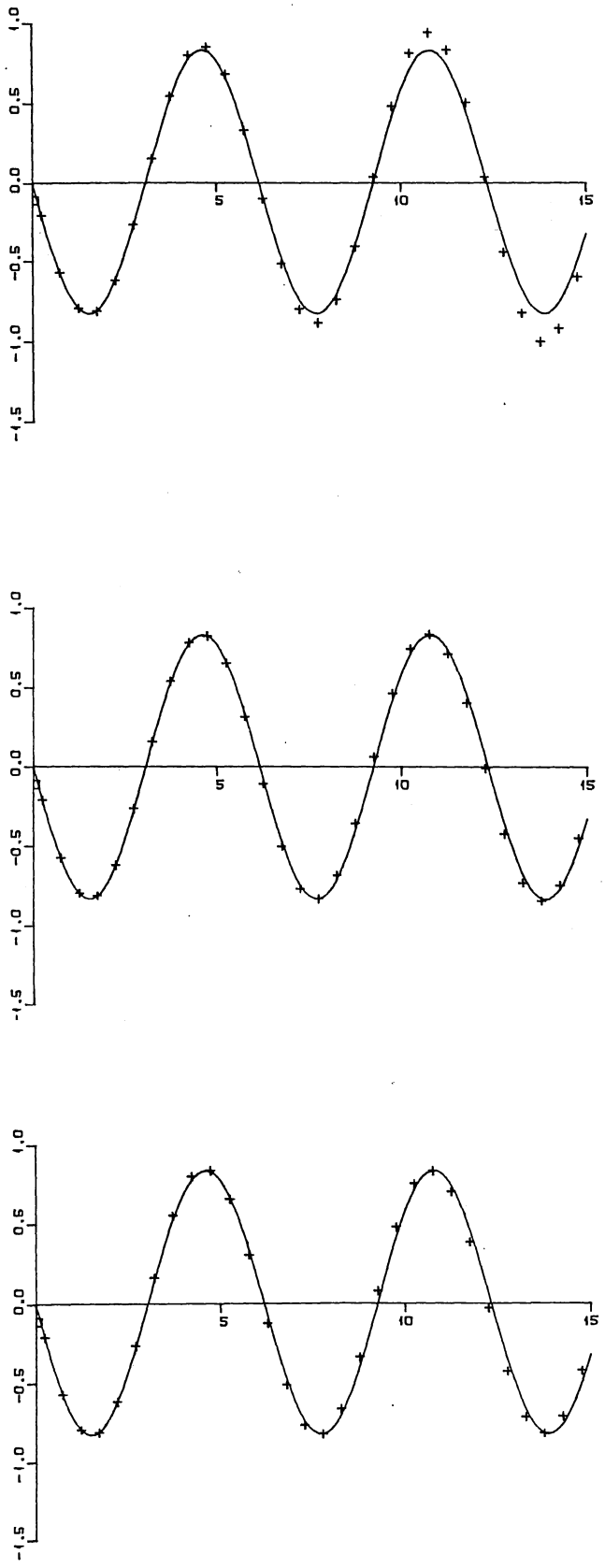

Figure 2.3

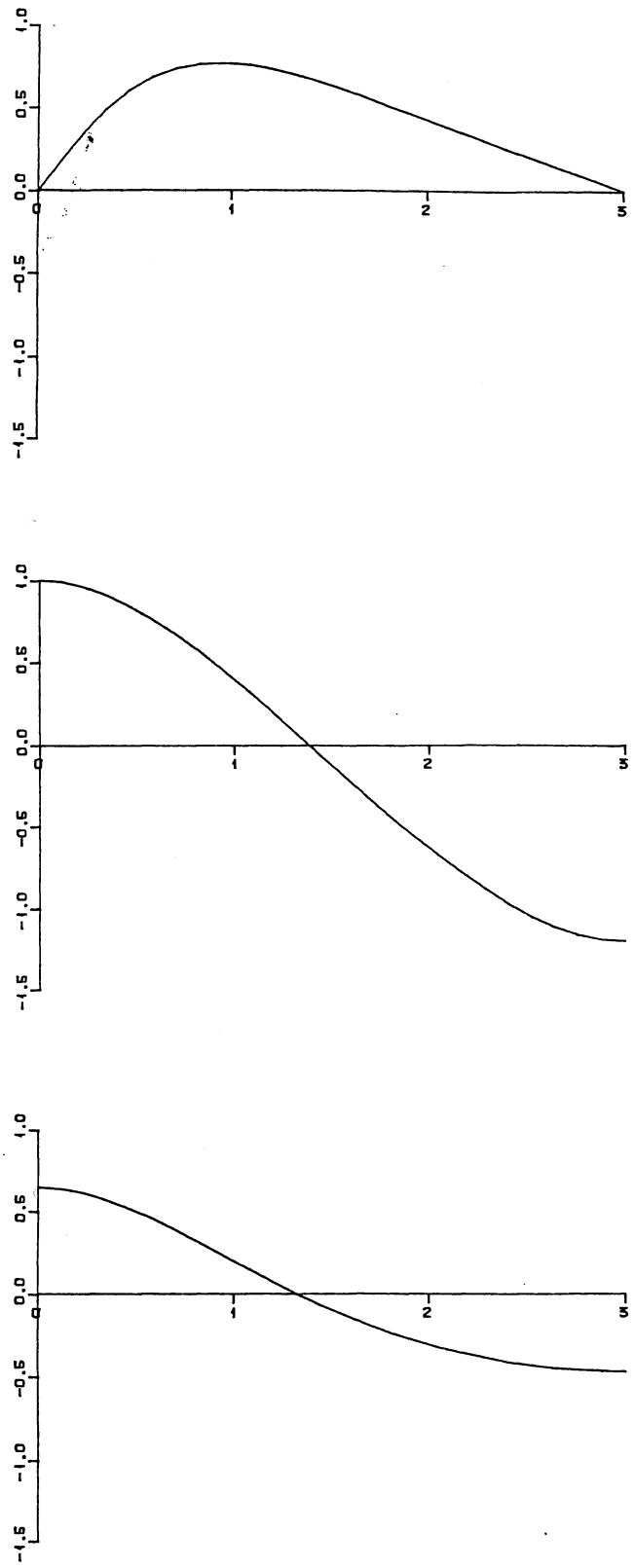

Figure 2.4

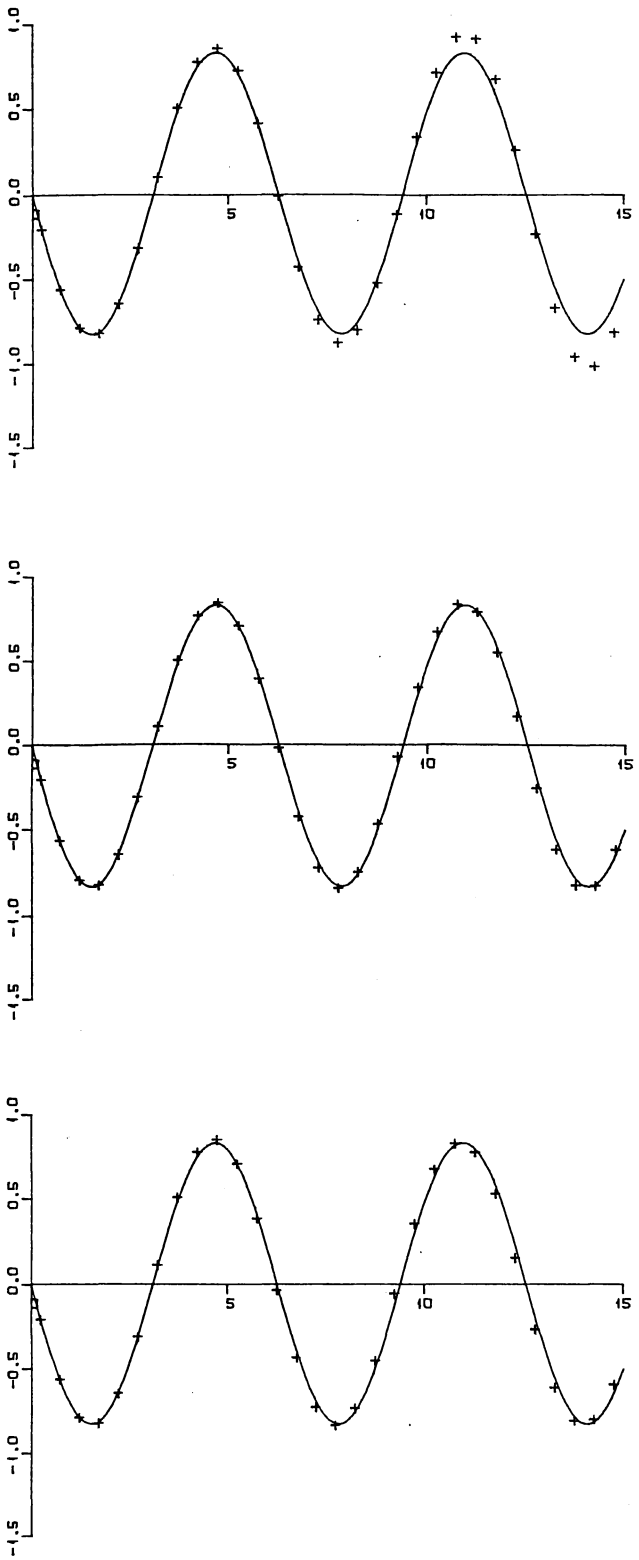

Figure 2.5

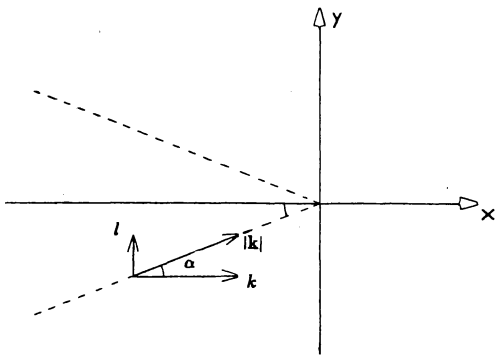

Figure 3.1

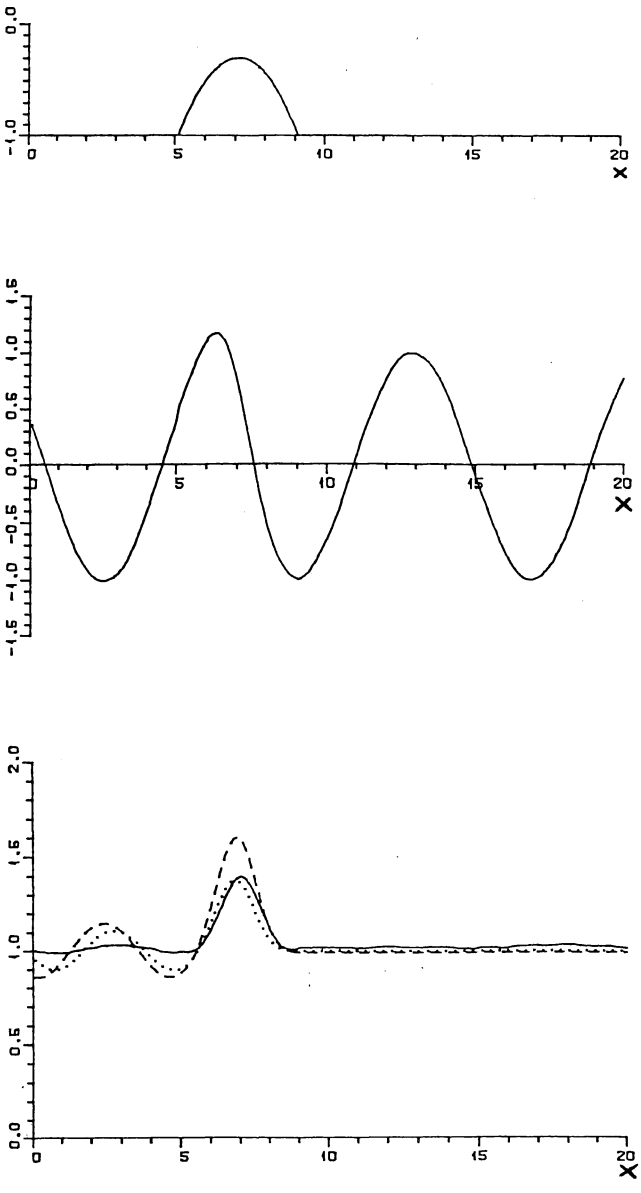

Figure 3.2

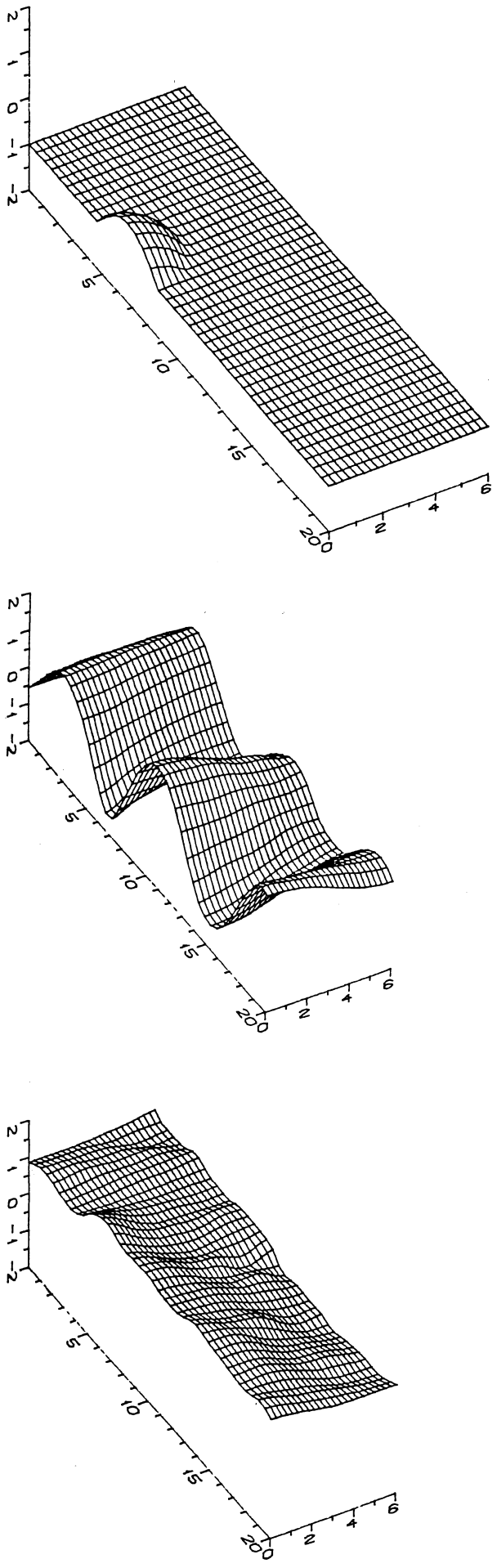

Figure 3.3

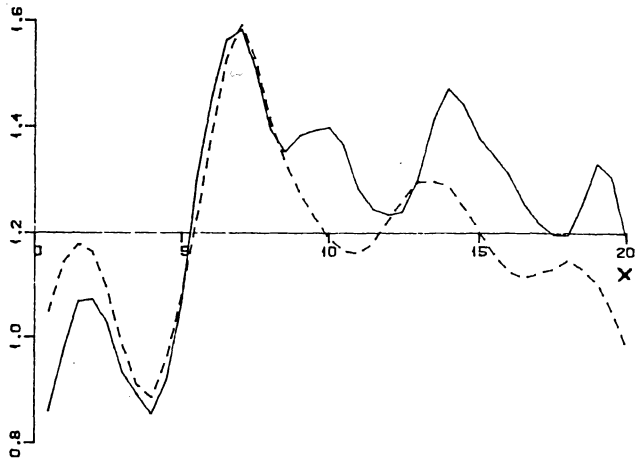

Figure 3.4

Table 4.1

Equations	$x = 63.9 \quad t = 100\Delta t$	$x = 221.0 \quad t = 250\Delta t$
(4.5)& (4.11)	0.09986	0.09976
(4.5)& (4.10)	0.09981	0.09969
(4.6)& (4.10)	0.09984	0.09973
(4.6)& (4.11)	0.09989	0.09980

Amplitude of the solitary wave after propagating a specified distance.
($\Delta x = 0.5,\ \Delta t = 0.5,\ \eta_0 = 0.1$)

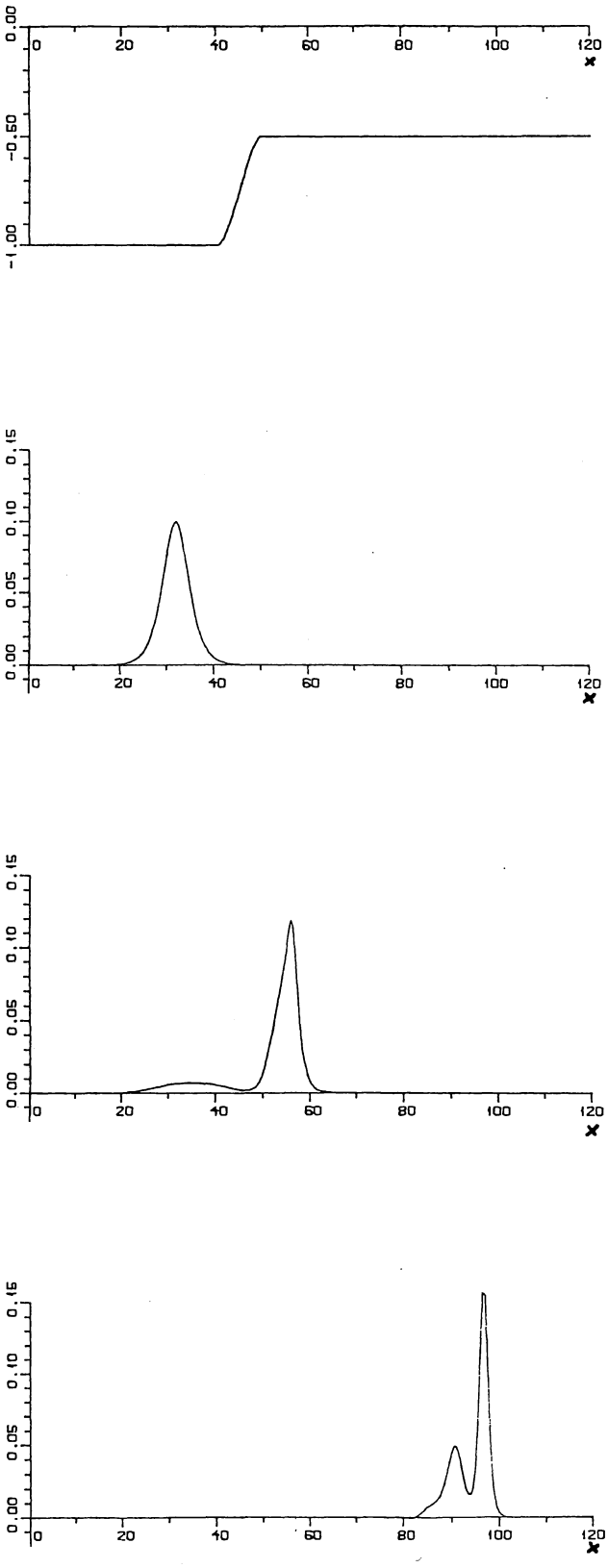

Figure 4.1

a) Initial conditions

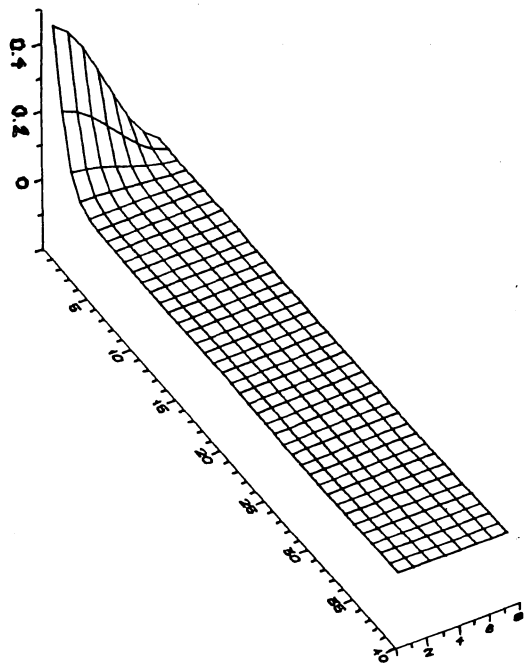

b) Nonlinear Boussinesq

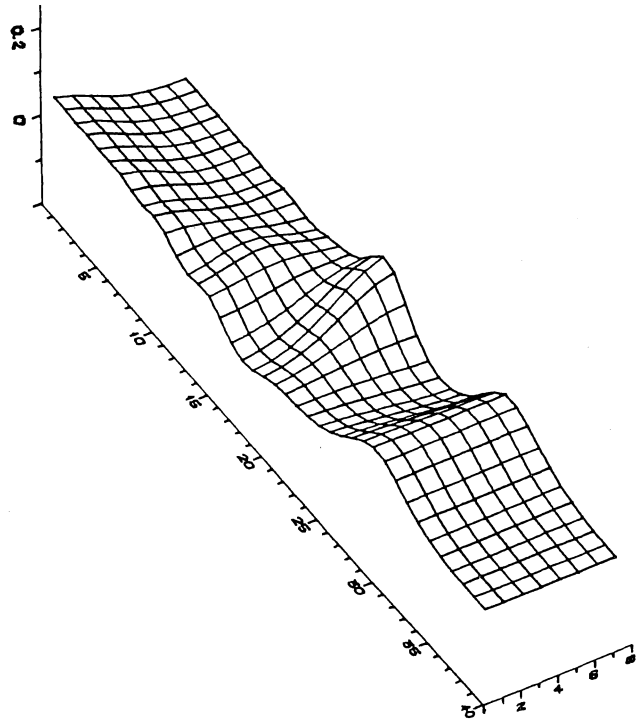

c) Linear Boussinesq

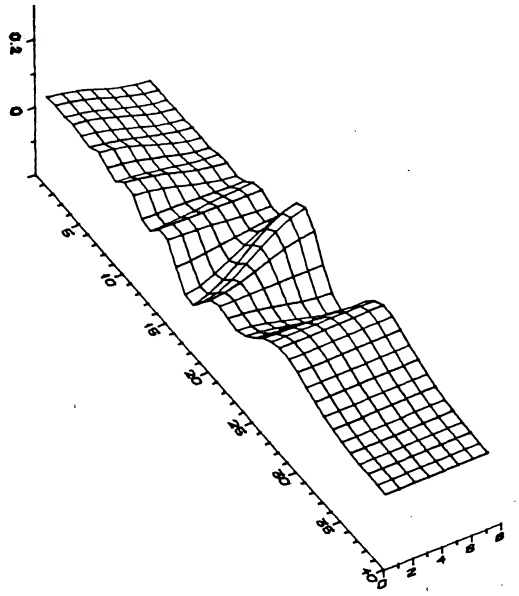

d) Hydrostatic

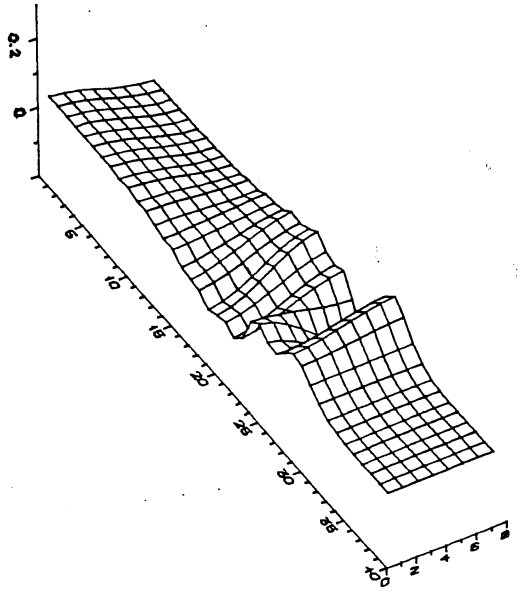

Figure 4.2

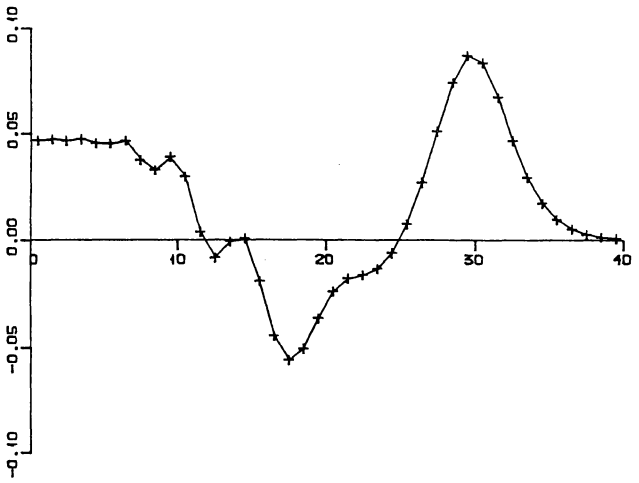

a) Nonlin. Bouss.
(—) 4 iter.
(++) 2 iter.

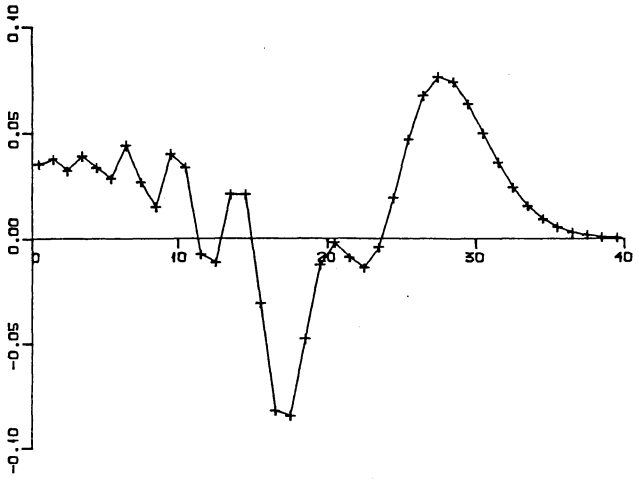

b) Lin. Bouss.
(—) 4 iter.
(++) 2 iter.

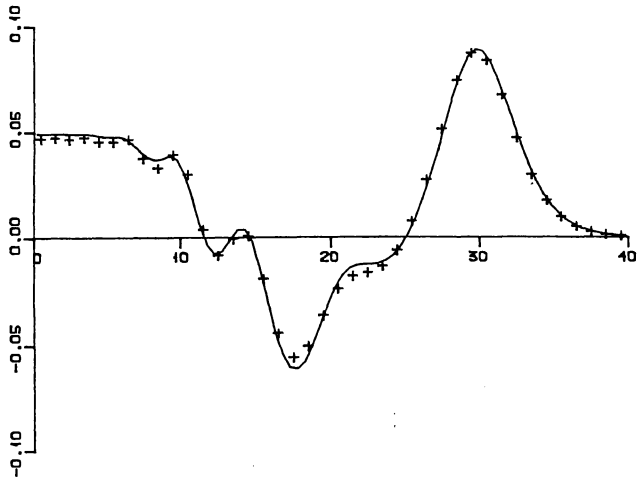

c) Nonlin. Bouss.
(—)$\Delta x = \Delta y = \Delta t = 0.5$
(++)$\Delta x = \Delta y = \Delta t = 1.$

Figure 4.3

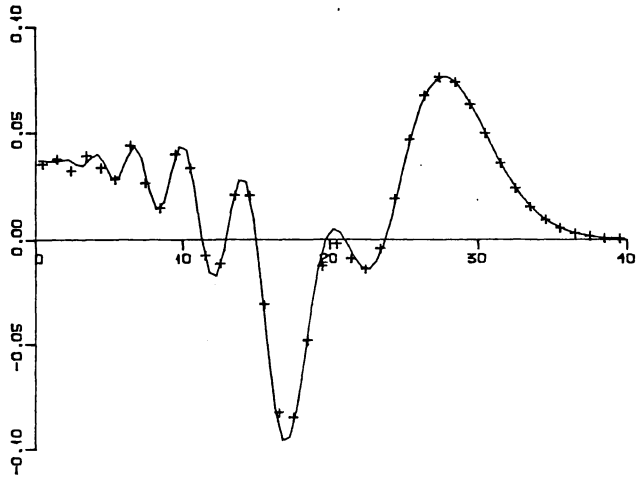

d) Lin. Bouss.
$(-)\Delta x = \Delta y = \Delta t = 0.5$
$(++)\Delta x = \Delta y = \Delta t = 1.0$

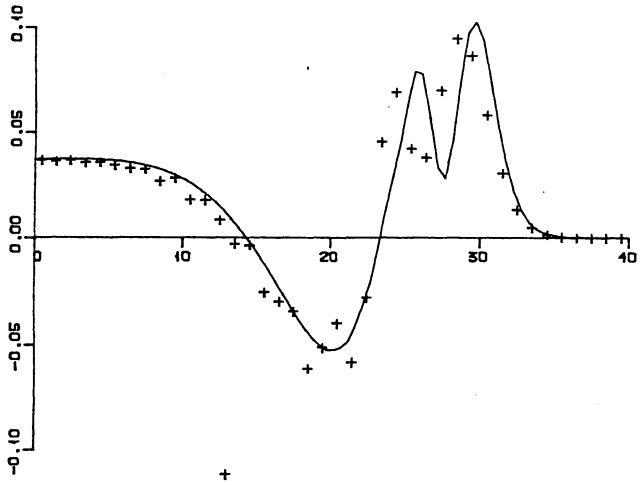

e) Hydrostatic. eq.
$(-)\Delta x = \Delta y = 0.5\ , \Delta t = 30/85$
$(++)\Delta x = \Delta y = 0.5\ , \Delta t = 30/43$

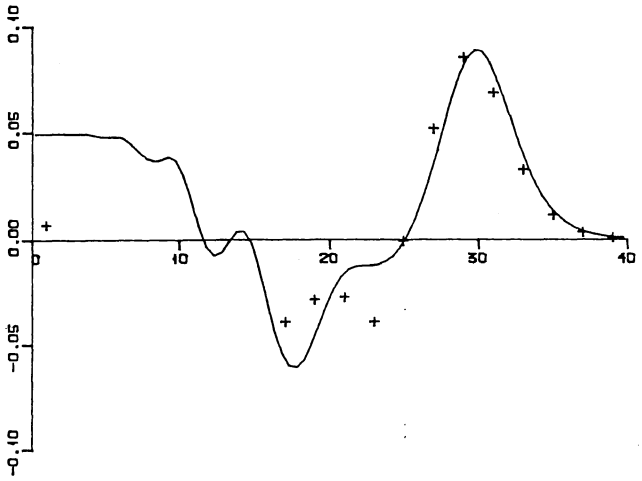

f) Nonlin. Bouss.
$(-)\Delta x = \Delta y = \Delta t = 0.5$
$(++)\Delta x = \Delta y = \Delta t = 2$

Figure 4.3

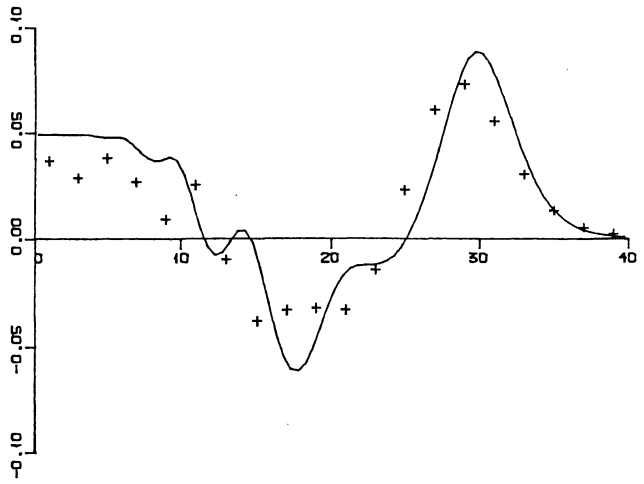

g) Nonlin. Bouss.
$(-)\Delta x = \Delta y = \Delta t = 0.5$
$(++)\Delta x = \Delta y = 2\ , \Delta t = 1.0$

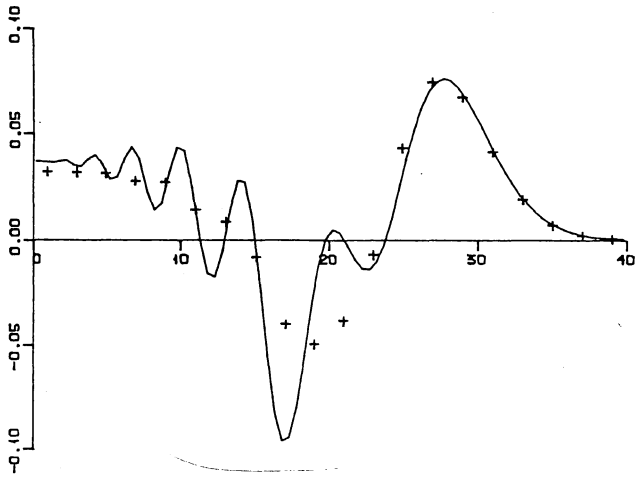

h) Lin. Bouss.
$(-)\Delta x = \Delta y = \Delta t = 0.5$
$(++)\Delta x = \Delta y = \Delta t = 2$

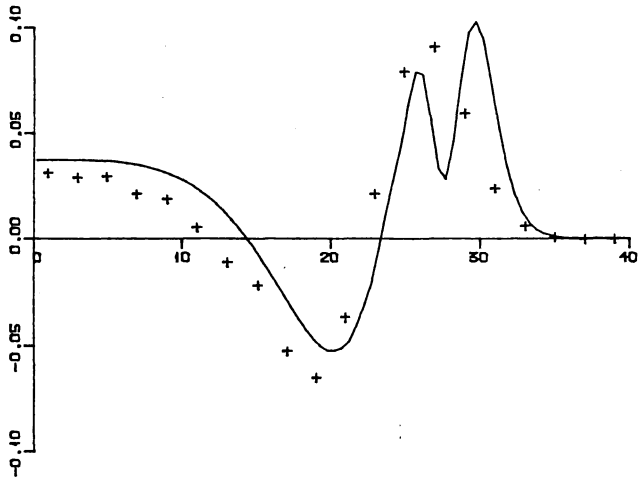

i) Hydrostatic eq.
$(-)\Delta x = \Delta y = \Delta t = 0.5$
$(++)\Delta x = \Delta y = \Delta t = 2$

Figure 4.3